

# Thin-Film Physics Group (Application-oriented thin-film research)

## 1 Epitaxial IV-VI narrow-gap semiconductor layers

M. Arnold, F. Felder, M. Rahim, A.N. Tiwari, and H. Zogg; www.tfp.ethz.ch

Epitaxial narrow gap lead chalcogenide (IV-VI) layers like  $\text{PbX}$ ,  $\text{Pb}_{1-y}\text{Sn}_y\text{X}$ ,  $\text{Pb}_{1-y}\text{Eu}_y\text{X}$  and  $\text{Pb}_{1-y}\text{Sr}_y\text{X}$  ( $\text{X}=\text{Te}$ ,  $\text{Se}$ ) are investigated for applications and basic research. The band gaps of the active infrared layers are between 0.1 and 0.25 eV (corresponding to wavelengths in the mid-IR range). Larger band gaps are realised with larger  $y$  values for the cladding  $\text{Pb}_{1-y}\text{Eu}_y\text{X}$  and  $\text{Pb}_{1-y}\text{Sr}_y\text{X}$  layers. All layers are grown by solid source molecular beam epitaxy (MBE) onto Si(111)-substrates by employing a  $\text{CaF}_2$  buffer layer, or onto  $\text{BaF}_2(111)$  substrates. The layers are heavily lattice- and (for Si-substrates) thermal-expansion mismatched. However, lead-chalcogenides are fault tolerant, and allow to realize high quality mid-infrared optoelectronic devices.

In addition, Bragg mirrors with very high reflectivity over a broad spectral range are easily obtained with a few quarter wavelength layers with alternating high and low refractive indices. With such mirrors Fabry-Perot cavities are formed.

### Resonant cavity enhanced detector (RCED)

By placing the active detector layer inside the cavity, a **resonant cavity enhanced detector (RCED)** is obtained. It is sensitive at the resonance wavelengths only where it exhibits a high quantum efficiency. The positions of the resonances are determined by the length of the cavity. In order to change the cavity length, the top mirror can be moved by micromechanical means. Such an arrangement forms a micro infrared spectrometer (**Fig. 1**). With a cavity length of  $\sim 15 \mu\text{m}$  this yields a spectral tuning range of  $0.6 \mu\text{m}$  at wavelengths around  $5 \mu\text{m}$ . Spectral width of the line is  $< 1\%$ .

A convenient way to describe the sensitivities (determined by the noise current densities) of photovoltaic infrared sensors are the  $R_0A$  products where  $R_0$  is the differential resistance of the current-voltage curve at zero bias and  $A$  is the diode area. **Fig.2** shows the absolute diffusion limits for bulk and thin absorbers, as well as the Shockley-Read generation/recombination for different lifetimes. For  $T > 200 \text{ K}$ , the measured  $R_0A$ -products are above the theoretical limit for an ideal bulk photodiode. This is due to the limited thickness (volume) of the active device part where S-R generation/recombination noise of charge carriers is possible. With RCED, it is therefore possible to obtain higher sensitivities compared to conventional (thick) photodiodes.

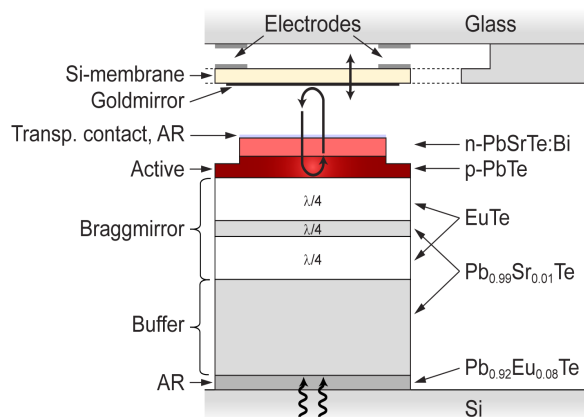


**Fig. 1:** Micromid-infrared spectrometer

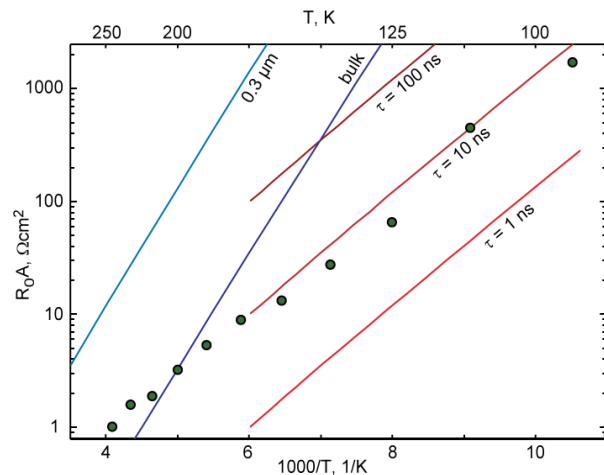


**Fig. 2:** Sensitivity ( $R_0A$  product) vs. temperature

### Vertical external cavity surface emitting laser (VECSEL)

VECSELs for the visible and near-infrared range are becoming popular due to their easy fabrication, scalability, and good beam quality. We realized the first VECSEL in the mid-infrared. The active layer is  $\text{PbTe}$  with emission wavelength around  $5 \mu\text{m}$ . It is optically pumped with a commercial laser diode with  $1.55 \mu\text{m}$  wavelength (**Fig. Z**). Light in/light out characteristics are shown in Fig. Z2. Multimode excitation is observed at higher pump powers, while at low power cw (continuous wave) emission is monomode. Maximum operation temperatures are presently 175K.

Similar VECSELS on Si(111) substrates are realized, too. Here, somewhat higher threshold powers are needed.

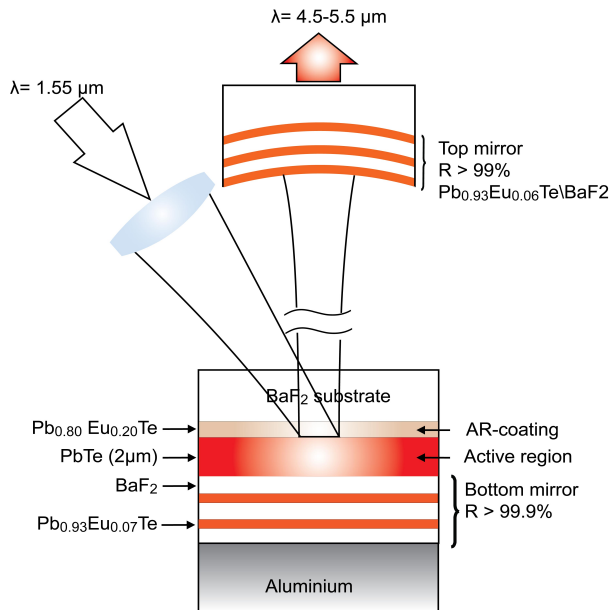


**Fig. 3:** Schematic representation of the IV-VI VECSEL. The curved DBR is used as output coupler.

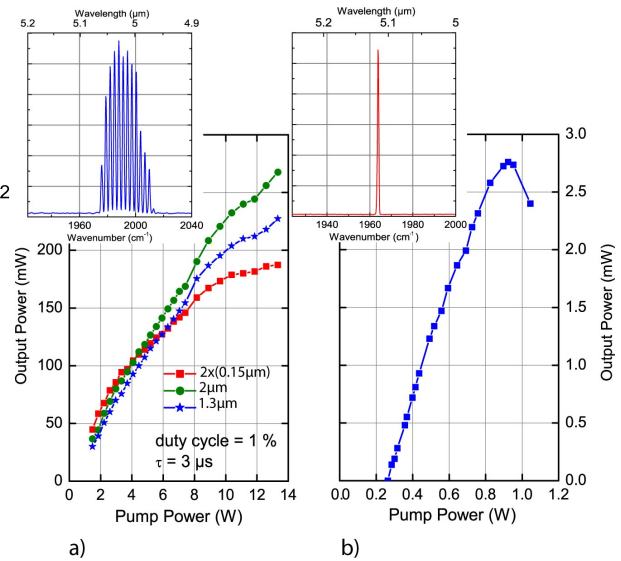


**Fig. 4:** Light-in/light-out characteristics at 100 K for pulsed (left) and CW excitation (right).

## 2 Thin-film solar cells based on Cu(In,Ga)Se<sub>2</sub> compound semiconductors

D. Brémaud, S. Bücheler, A. Chirila, S. Seyrling, R. Verma, H. Zogg, and A.N.Tiwari; [www.tfp.ethz.ch](http://www.tfp.ethz.ch)

Safe, cheap, abundant, renewable, and environment-friendly generation of electricity is of considerable interest for our society. Thin-film solar cell technology based on the polycrystalline compound semiconductor Cu(In,Ga)Se<sub>2</sub> (usually abbreviated as "CIGS") is a very promising solution for this task. New cell concepts to improve the stability and efficiency are among further projects.

### High Growth Rate CIGS layers

Deposition of the CIGS absorber layer in the solar cell by elemental co-evaporation is the currently slowest and one of the most expensive processing steps. Optimizing and simplifying this processing step in terms of increasing the growth rate will provide guidelines for cost-effective industrial production. Development of a suitable growth process requires investigation of the influence of process parameters on structural, compositional, electronic properties of layers and solar cells. We have scaled down our 45 min long state-of-the-art process which yielded a best efficiency of 15.3% to a 20 min long process that yielded 13.2%.

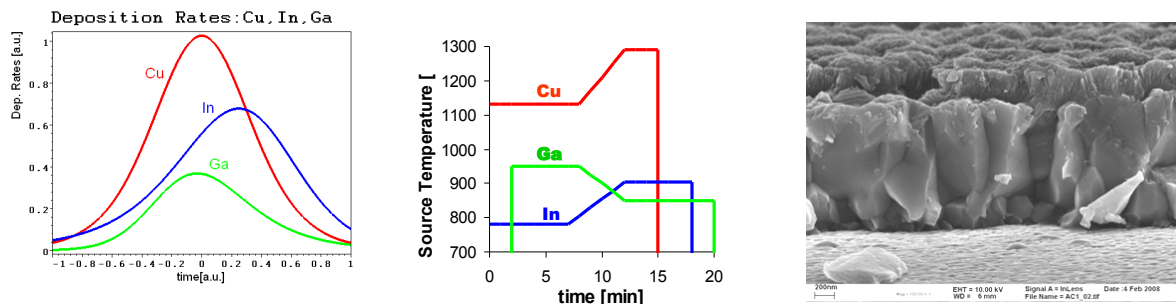


**Fig. 5:** Left: Simulated in-line deposition process. Middle: Applied first-order approximation of the simulation. Right: SEM cross section of finished solar cells with CIGS grown in 20 min.

## In<sub>2</sub>S<sub>3</sub> Buffer layers deposited by physical vapor deposition

Physical vapor deposition was employed to deposit In<sub>2</sub>S<sub>3</sub> buffer layers on CIGS absorber. The buffer layers were grown by evaporation of In<sub>2</sub>S<sub>3</sub> powder as a source material. The microstructural behavior and chemical composition of the source materials as a function of the time of evaporation have been studied. A significant amount of sulfur loss was detected in coarse powder, while the finer powder was found to be chemically stable. Solar cells made of a buffer layer deposited from fine powder resulted in lower efficiency (8.6%) than that made from coarse powder (11.6%). A highly efficient solar cell of 14.1% efficiency was developed with a ~60 nm thin In<sub>2</sub>S<sub>3</sub> buffer layer.

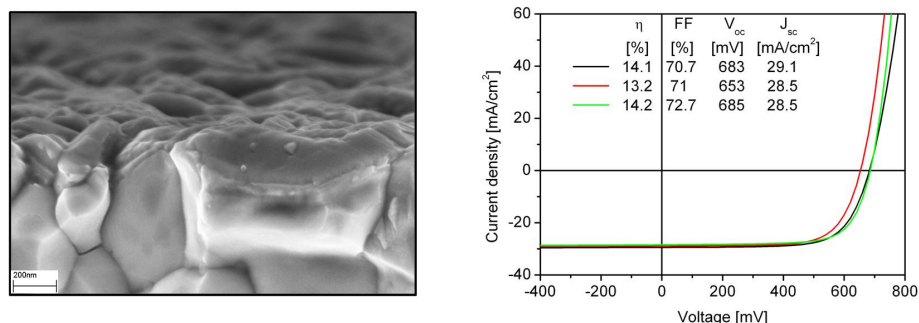


**Fig. 6:** Left: a uniform coverage of a ~30 nm thick evaporated In<sub>x</sub>S<sub>y</sub> layer on CIGS was clearly distinguishable in the SEM cross-section image. Right: J-V characteristic of solar cell with 60 nm thin In<sub>x</sub>S<sub>y</sub> buffer layer: (-----) as-grown; (- - - -) cell air annealed for 5 min at 200 °C and, (- - - -) CBD-CdS reference cell.

## Nanocrystalline dye-sensitized / Cu(In,Ga)Se<sub>2</sub> tandem solar cells

The opto-electronic properties of Cu(In,Ga)Se<sub>2</sub> (CIGS) absorbers, especially the high photon absorption even at longer wavelengths (> 900 nm) and the possibility to adapt the band gap of the semiconductor from 1.04 eV to 1.67 eV, makes them highly attractive candidates for the bottom cell in a tandem configuration. In collaboration with EPFL we used a novel concept of nanocrystalline dye sensitized solar cells as a top cell for the conversion of the high energy photons (wavelengths of 350 - 700 nm) and applied a CIGS solar cell as the bottom cell for the remaining unabsorbed photons of wavelengths > 700 nm. The resulting tandem solar cell shows a conversion of 15.1 % under AM1.5 illumination and further potential for efficiency improvement.

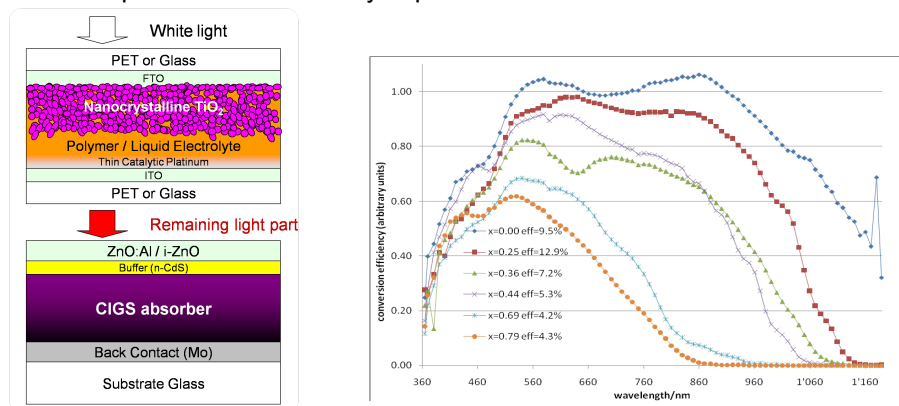


**Fig. 3:** Left: Schematic configuration of the mechanical stack of top nanocrystalline dye and bottom CIGS tandem solar cell showing various device layers. Right: Quantum efficiency of CIGS cells with different Ga contents to adapt the band gap.